European Conference on Computational Fluid Dynamics
ECCOMAS CFD 2006
P. Wesseling, E. Oñate and J. Périaux (Eds)

A COMPARISON OF AN ENTHALPY AND A TEMPERATURE METHOD FOR MELTING PROBLEMS ON COMPOSITE DOMAINS

J.H. Brusche*, A. Segal*, C. Vuik* and H.P. Urbach†

*Delft University of Technology, Faculty EWI
Mekelweg 4, 2628 CD, The Netherlands
e-mail: [j.h.brusche, a.segal, c.vuik]@tudelft.nl

†Philips Research Laboratories
Professor Holstlaan 4, 5656 AA Eindhoven, The Netherlands
e-mail: h.p.urbach@philips.com

Key words: Stefan problem, Enthalpy method, Temperature method, Optical rewritable recording

Abstract. *In optical rewritable recording media, such as the Blu-ray Disc, amorphous marks are formed on a crystalline background of a phase-change layer, by means of short, high power laser pulses. It is of great importance to understand the mark formation process, in order to improve this data storage concept. The recording layer is part of a grooved multi-layered geometry, consisting of a variety of materials of which the material properties are assumed to be constant per layer, but may differ by various orders of magnitude in different layers. The melting stage of the mark formation process requires the inclusion of latent heat. In this study a comparison is made of numerical techniques for resolving the associated Stefan problem. The considered methods have been adapted to be applicable to multi-layers.*

1 INTRODUCTION

In optical rewritable recording, a disk consists of various layers. The actual recording of data, stored as an array of amorphous regions in a crystalline background, takes place in a specific layer of the recording stack. This layer consists of a so-called phase-change material. The amorphous regions, called marks, are created as a result of very short high intensity pulses of a laser beam that is focused on this active layer. The light energy of the laser is transformed into heat, which locally causes the phase-change material to melt. As soon as the laser is switched off, the molten material solidifies. At the same time, recrystallization occurs in those regions where the temperature is below the melting temperature, but still above the recrystallization temperature. Since the cooling down is very rapid (quenching), almost no recrystallization occurs within the molten region, and

thus a solid amorphous area is formed. The same laser beam, but at a lower power level, can be used in a similar way to fully recrystallize the amorphous regions. The recorded data is then erased.

To ensure that the optical system knows its exact location on the disk at all time, a rewritable disk contains a concentric, outwards spiraling groove. Modulations in the refracted light, as a result of the grooves, are processed to position the optical head (tracking). In radial direction, a periodic 'land and groove' structure can thus be discerned. For a Blu-ray recording stack, a typical configuration is depicted in Figure 1.

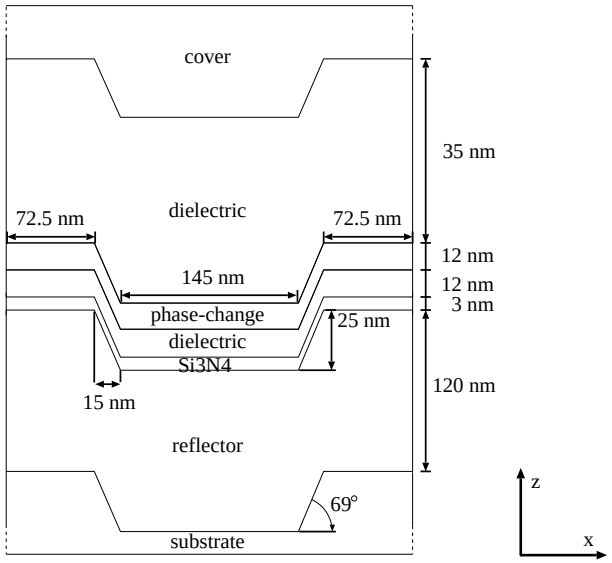

Figure 1: Sketch of a typical recording stack for a Blu-ray disk.

Although much is understood about the concept of optical rewritable recording, many open questions remain. In order to gain better inside in for instance the influence of polarization and wavelength of the incident light or the geometry and composition of the stack on the shape and position of a mark, robust (numerical) modeling is essential. As a result, the occurrence of unwanted effects, such as cross-track cross-talk, can be minimized.

In this study we will focus on the melting phase of the mark formation process. In contrast to earlier work[1], this requires the contribution of latent heat to be taken into account in the computation of the temperature distribution in the optical recording disk. The mathematical model associated with the melting problem will be presented first. Two numerical techniques to resolve the mathematical problem will then be introduced. Emphasize is put on how these methods can be applied to multi-layered domains. Finally, a comparison with respect to accuracy, convergence behavior and computational demand is presented. For convenience, we will restrict ourselves to 1D and 2D test problems only.

2 PROBLEM DESCRIPTION

The melting of the phase-change material is a complex process. Material specific properties, such as the latent heat, greatly influence the melting behavior. Therefore, some assumptions are made with respect to several physical aspects of the melting process. First of all, it is assumed that the melting of the phase-change material occurs at a melting *point* T_m, rather than along a melting trajectory. In this way, the shape and size of mark are simply determined by the (sharp) moving interface between the solid and liquid state of the (crystalline) phase-change material. Furthermore, the density ρ, latent heat L, heat capacity c, and conductivity κ are taken to be constant per phase. When needed, a subscript s or l is used to distinct between the solid and liquid state, respectively.

Because the position of the moving interface evolves in time, depending on the heat distribution, the melting process is modeled as a moving boundary problem. For an arbitrary domain $\Omega \subset \mathbb{R}^n$ with fixed outer boundary $\delta\Omega$ and moving boundary $\Gamma(t)$, leading to two sub-domains Ω_s and Ω_l such that $\bar{\Omega} = \bar{\Omega}_s \cup \bar{\Omega}_l$ and $\Omega_s \cap \Omega_l = \emptyset$, the two-phase Stefan problem is given by:

$$\begin{cases} \rho c_{s,l} \dfrac{\partial T(x,t)}{\partial t} = \kappa_{s,l} \Delta T(x,t) + q(x,t) & \forall x \in \Omega_{s,l}, t > 0 \quad \text{(1a)} \\ \rho L v_n = \left[\kappa_{s,l} \dfrac{\partial T(x,t)}{\partial n} \right], \quad T(x,t) = T_m & \text{for } x = \Gamma(t), t \geq 0 \quad \text{(1b)} \\ T(x,0) = \bar{T}_1(x) & \forall x \in \Omega_{s,l} \quad \text{(1c)} \end{cases}$$

where n denotes the unit normal vector on the moving interface pointing from the solid domain into the liquid domain, and v_n is the velocity of the moving interface, together with one or more of the following boundary conditions on the complementary parts $\delta\Omega_i, i = 1, 2, 3$ of the fixed outer boundary $\delta\Omega = \bigcup_{i=1}^{3} \delta\Omega_i$:

1. A Dirichlet condition on $\delta\Omega_1$:
$$T = \bar{T}_2(x). \tag{2}$$

2. A Neumann condition on $\delta\Omega_2$:
$$\kappa_{s,l} \frac{\partial T}{\partial n}(x) = \bar{q}(x), \tag{3}$$
where $\bar{q}(x)$ is a given normal heat flux.

3. A radiation-type boundary condition on $\delta\Omega_3$:
$$\kappa_{s,l} \frac{\partial T}{\partial n}(x) = \bar{\alpha}(T), \tag{4}$$
where $\bar{\alpha}(T)$ is a function of temperature.

At $t = 0$ the whole domain is taken to be solid. By $[\phi]$ we denote the jump in ϕ defined as:

$$[\phi] = \lim_{\substack{x \longrightarrow \Gamma(t) \\ x \in \Omega_s(t)}} \phi(x,t) - \lim_{\substack{x \longrightarrow \Gamma(t) \\ x \in \Omega_l(t)}} \phi(x,t). \tag{5}$$

3 TWO APPROACHES TO THE STEFAN PROBLEM

Two fixed grid approaches to solve the Stefan problem given above can be distinguished: the *enthalpy* formulation and the *temperature* formulation. Under the above-mentioned assumptions, the enthalpy $H(T)$ can be defined as:

$$H(T) = \begin{cases} \rho c_s (T - T_m), & T \leq T_m \\ \\ \rho c_l (T - T_m) + \rho L, & T > T_m \end{cases} \tag{6}$$

In the enthalpy formulation the enthalpy H is treated as a second dependent variable besides the temperature T. Using relation (6), the heat conduction equation (1a) and the Stefan condition (1b) are replaced by the well-known enthalpy equation:

$$\frac{\partial H(T)}{\partial t} - \kappa_{s,l} \Delta T = q. \tag{7}$$

In the temperature formulation, instead of separating the domain in a liquid and solid part, as via definition (6), the enthalpy is written according to its formal definition: as the sum of sensible and latent heat:

$$H(T) = H^{\text{sensible}} + H^{\text{latent}} = \rho c_{s,l} (T - T_m) + \rho L f_l(T), \tag{8}$$

where $f_l(T)$ denotes the liquid volume fraction, which in case of isothermal phase-change is equal to the Heavyside step function $\mathcal{H}(T - T_m)$. Definition (8) leads to the classical Fourier heat conduction equation, but with an additional term for the latent heat contribution:

$$\rho c_{s,l} \frac{\partial T}{\partial t} + \rho L \frac{\partial f_l}{\partial t} - \kappa_{s,l} \Delta T = q. \tag{9}$$

Here, the time derivative of the liquid volume fraction is to be interpreted in the weak sense.

4 NUMERICAL METHODS

The resolution of the Stefan problem (1a-1c) by means of a numerical method is not trivial. On the one hand, the method should be applicable to multi-layered domains, with possibly large jumps in physical parameters. In addition, there are variations in the geometry (i.e., the grooved tracks), in three dimensional space. These demands also make that a finite element discretization is preferred. On the other hand, the method should allow

for the breaking and merging of interfaces, as a result of for instance the inhomogeneity of the internal heating by the laser or the applied multi-pulse strategy. Furthermore, a future generalization of the method (e.g., non-isothermal melting; temperature dependent material properties) should be possible.

Two numerical approaches to resolve the Stefan problem (1a-1c) are described next. The first method is based on the work by Nedjar[4], in which a relaxed linearization of the temperature is used to solve the enthalpy equation (7). The governing equation for the second method is the temperature formulation (9). Key to this approach is the discontinuous integration across elements that are intersected by the moving boundary, as proposed by Fachinotti et al.[3].

4.1 Relaxed linearization

By means of the standard Galerkin finite element method, a system of (nonlinear) equations that is equivalent to the enthalpy equation (7), in combination with one or more of the boundary conditions (2)-(4), is given in matrix-vector notation by:

$$M\frac{\partial H}{\partial t} + ST = q, \tag{10}$$

where M is the mass matrix and S is the stiffness matrix.

In case Euler backward is applied for the time integration, with a time step size Δt, the fully discretized system at time level $m+1$ is given by:

$$M\frac{H^{m+1} - H^m}{\Delta t} + ST^{m+1} = q^{m+1}. \tag{11}$$

Remark that, for simplicity, the time-dependency of the stiffness matrix, which is not constant because the position of the moving interface determines the value of the diffusivity κ for each node at each time level, has been omitted. The mass matrix is always constant, since the conductivity c is contained in the enthalpy.

Nedjar[4] describes how the fully discretized system (11) can be solved using a pseudo-Newton iterative procedure in terms of a temperature increment ΔT_i. Before we explain how this technique can be adapted to solve for the temperature distribution in a multi-layered domain, we will first briefly repeat the three steps that form the key idea behind the proposed integration algorithm by Nedjar[4]. We conclude this section with an evaluation of the presented method with respect to the mark formation model.

First, introduce the reciprocal function $\tau : \mathbb{R} \longrightarrow \mathbb{R}$ of (6), given by $T = \tau(H)$ and define

$$H_{i+1} = H_i + \Delta H_i, \tag{12}$$

$$T_{i+1} = T_i + \Delta T_i. \tag{13}$$

Next, consider a linearization of the function $\tau(H)$:

$$T_{i+1} = T_i + \Delta T_i = \tau(H_i) + \tau'(H_i)\Delta H_i, \tag{14}$$

or, rewritten in terms of the enthalpy update ΔH_i:

$$\Delta H_i = \frac{1}{\tau'(H_i)} \left[\Delta T_i + (T_i - \tau(H_i))\right]. \tag{15}$$

Here, τ' denotes the derivative of τ with respect to its argument. Unfortunately, this derivative can be zero. This is resolved by approximating the fraction in equation (15) by a constant μ defined as:

$$\mu = \frac{1}{\max(\tau'(H_i))}, \tag{16}$$

such that the relaxed enthalpy update becomes:

$$\Delta H_i = \mu \left[\Delta T_i + (T_i - \tau(H_i))\right]. \tag{17}$$

If we now define

$$\tilde{q} = q^{m+1} + \tilde{M} H^m, \qquad \tilde{M} = \frac{1}{\Delta t} M, \tag{18}$$

then substitution of (12)-(14) and (17) into the discretized system (11) gives:

$$\tilde{M} \left\{H_i + \mu \left[\Delta T_i + (T_i - \tau(H_i))\right]\right\} + S(T_i + \Delta T_i) = \tilde{q}. \tag{19}$$

A rearrangement of terms finally leads to

$$\left(\mu \tilde{M} + S\right) \Delta T_i = \tilde{q} - \left(\mu \tilde{M} + S\right) T_i - \tilde{M} \left(H_i - \mu \tau(H_i)\right). \tag{20}$$

By rewriting the discretized heat conduction equation in terms of the temperature increment ΔT_i for those layers of a recording stack that do not contain a phase change material, it is possible to build a system of equations for the multi-layer as a whole. This means, that any existing finite element code for heat conduction problems in composite domains, can easily be extended to include melting.

4.2 Discontinuous integration

A distinct feature of a temperature based model such as (9), is the use of discontinuous spatial integration. The key idea behind discontinuous integration, as for instance described by Fachinotti et al.[3] is that for elements intersected by the moving interface, the integrals arising from a finite element discretization of the governing equation (9) are computed over the liquid and solid part separately. Because no regularization of the integrand is required, an accurate evaluation of the discrete balance equation is assured.

The application of the general Galerkin procedure, in which we approximate the temperature field by

$$T(\mathbf{x}, t) \approx \sum_{i=1}^{n} \phi_i(\mathbf{x}) T_i(t), \tag{21}$$

where ϕ_i is a (linear) basis shape function and T_i is the nodal temperature, and using Euler backward time discretization, lead to the following discretized system of (nonlinear) equations (at time level $m+1$):

$$M^{m+1}\frac{T^{m+1}-T^m}{\Delta t}+\frac{L^{m+1}-L^m}{\Delta t}+S^{m+1}T^{m+1}=q^{m+1}. \tag{22}$$

Note that, when compared to the enthalpy approach, both the mass matrix as well as the stiffness matrix are now time-dependent.

The matrix and vector entries for the above system are given by (boundary conditions have been omitted):

$$M_{ij}=\int_\Omega \rho c\phi_i\phi_j d\Omega, \tag{23}$$

$$S_{ij}=\int_\Omega \nabla\phi_i\cdot(\kappa\nabla\phi_j)d\Omega, \tag{24}$$

$$L_i=\rho L\int_\Omega \phi_i f_l d\Omega, \tag{25}$$

$$q_i=\int_\Omega \phi_i q d\Omega. \tag{26}$$

The heat conduction equation (9) is highly nonlinear, due to the addition of the latent heat term $\frac{\partial f_l}{\partial t}$. In practice, the solution to the corresponding discretized system of equations (22) can be found by either using Picard iterations or by use of Newton-Raphson.

Let us consider the residual form of the system of equations (22):

$$\Psi(T^{m+1})=M^{m+1}\frac{T^{m+1}-T^m}{\Delta t}+\frac{L^{m+1}-L^m}{\Delta t}+S^{m+1}T^{m+1}-q^{m+1}=0. \tag{27}$$

Starting with an initial guess $T_0^{m+1}=T^m$, the subsequent approximations of the solution $T_i^{m+1}, i=1,2,\ldots$ to (27), by means of Picard iterations, are computed via:

$$T_i^{m+1}=\Psi(T_{i-1}^{m+1}). \tag{28}$$

Unfortunately, for our application, this basic iterative scheme hardly ever leads to convergence: in most cases 'flip-flop', in which the solution jumps between two different states, is observed. A means of improving the convergence behavior is the use of weighted under-relaxation:

$$T_i^{m+1}=T_{i-1}^{m+1}+\omega\left[\Psi(T_{i-1}^{m+1})-T_{i-1}^{m+1}\right]. \tag{29}$$

The problem with this approach is that we do not know any means of selecting an optimal value for ω, other than by trial-and-error. Furthermore, if a certain value of ω

improves convergence for one time step, this does not automatically guarantee it will also improve the convergence for subsequent time steps.

The main advantage of the Newton-Raphson iterative scheme is that locally quadratic convergence is assured, as soon as the norm of the difference between the numerical solution and the exact solution is less than the radius of convergence. For the ith iterate of the Newton-Raphson scheme we have:

$$T_i^{m+1} = T_{i-1}^{m+1} + \Delta T_{i-1}^{m+1}, \tag{30}$$

where ΔT_{i-1}^{m+1} is the solution of the linear system

$$J(T_{i-1}^{m+1})\Delta T_{i-1}^{m+1} = -\Psi(T_{i-1}^{m+1}). \tag{31}$$

The Jacobian J is given by

$$J(T_{i-1}^{m+1}) = \frac{\partial \Psi}{\partial T} = \frac{1}{\Delta t}\left(M^{m+1} + \frac{\partial L}{\partial T}\right) + S^{m+1}. \tag{32}$$

The partial derivative of L with respect to the temperature T needs special attention. Following the definition of $L_i^{e_i}$ it is easily derived that

$$\frac{\partial L_i^{e_i}}{\partial T_j} = \rho L \int_{\Omega^{e_i}} \frac{\partial H(T - T_m)}{\partial T_j}\phi_j d\Omega^{e_i} \tag{33}$$

$$= \rho L \int_{\Omega^{e_i}} \delta(T - T_m)\phi_i\phi_j d\Omega^{e_i}. \tag{34}$$

It is shown in Fachinotti[3] that the integral (34) over Ω^{e_i}, at the finite element level, can be rewritten as an integral over the segment of the interface Γ^{e_i} contained in element e_i:

$$\rho L \int_{\Omega^{e_i}} \delta(T - T_m)\phi_i\phi_j d\Omega^{e_i} = \rho L \int_{\Gamma^{e_i}} \frac{\phi_i\phi_j}{\|\nabla T\|} d\Gamma^{e_i}. \tag{35}$$

As with the Picard iterations, in practice, divergence of the Newton-Raphson scheme is often observed when highly nonlinear problems are considered. In particular, this concerns problems for which the latent heat is relatively large in comparison to the other physical parameters. The reason for the non-convergence of the Newton-Raphson scheme is that the computed Newton step ΔT_{i-1}^{m+1} is too large.

A reasonable strategy to counteract this problem, is to perform a line search along the Newton direction. The temperature is then updated via:

$$T_i^{m+1} = T_{i-1}^{m+1} + \alpha \Delta T_{i-1}^{m+1}, \tag{36}$$

The scaling parameter α can for instance be determined using quadratic regression.

In the temperature based formulation (9), the term representing the latent heat contribution can be interpreted as an additional source for the classical heat conduction equation. Therefore, the discontinuous integration method can be easily included in any existing finite element code for multi-layered domains, to incorporate melting.

5 NUMERICAL EXPERIMENTS

The two methods presented in the previous section have been applied to some 1D test problems. A 2D test problem is also considered. A comparison is made of the performance of both methods with respect to number of iterations and computational time for varying time step size Δt and number of elements n. Since the numerical method should be applicable to a wide range of materials, performance is also compared for varying Stefan numbers $St = c_l(T_0 - T_m)/L$. Here, c_l is the conductivity of the liquid phase and T_0 the ambient temperature.

For both methods the time step size is chosen to be such, that at all time instances, the moving interface changes at most from the originally intersected elements to adjacent elements. In this way it is ensured that the contribution of latent heat is taken into account appropriately.

The error in the numerical solution T_n with respect to the analytical solution T_{ana} is determined as:

$$\text{error} = \frac{\|T_{\text{ana}} - T_n\|_k}{\|T_{\text{ana}}\|_k} \times 100\%. \tag{37}$$

Here, the subscript n refers to the number of elements used to approximate the solution. The type of norm used to measure the error is indicated by the subscript k. Both the 2-norm and ∞-norm will be considered. The error is computed for both the temperature as a function of time, at a fixed node located at $x = 0.3$m (*error 1*), as well as the temperature as a function of position, at $t = t_{\text{end}}$ (*error 2*). In the tables, the errors 1 and 2 are given in both the 2-norm and $\infty-$norm (within brackets).

In the method of Nedjar, a linear system for the temperature update ΔT is solved. In the Fachinotti method, a non-linear system for T^{m+1} is solved. Both systems are solved

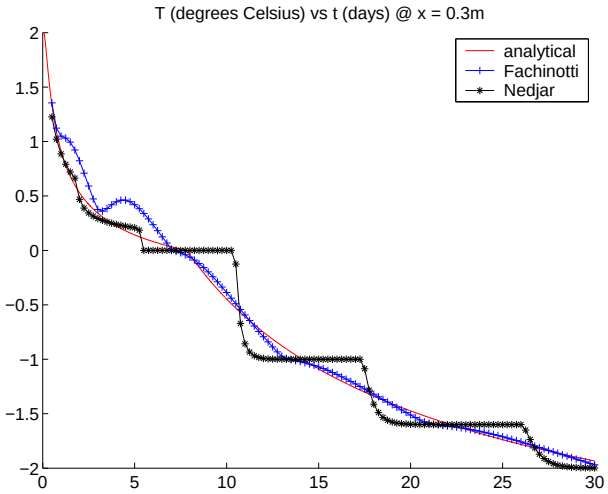

Figure 2: Test case 'equal': Difference between Nedjar and Fachinotti for the temperature as function of time in a point $x = 0.3$m. $n = 100$, $\epsilon = 10^{-6}$.

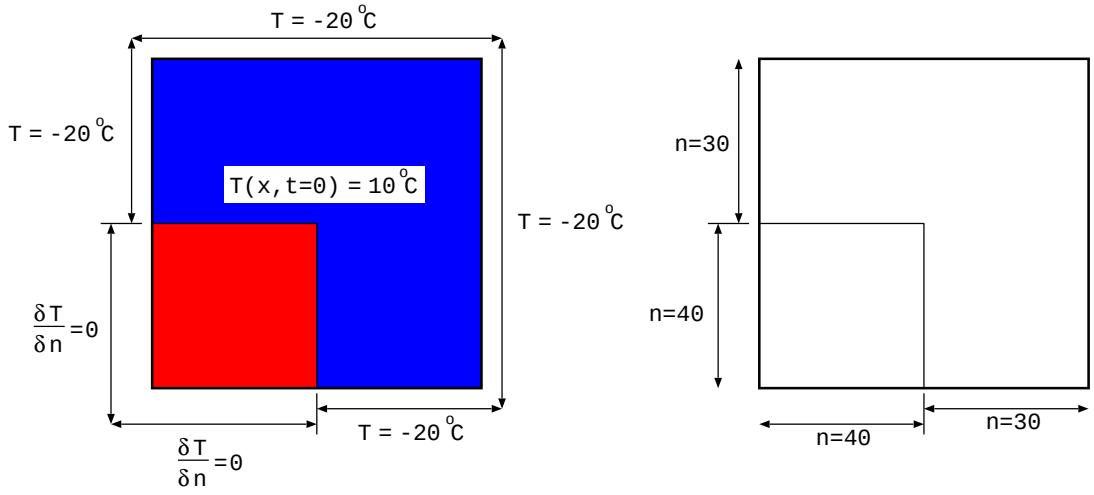

Figure 3: 2D test case: initial and boundary conditions (left). Number of grid points used (right).

iteratively, but the stopping criterion for each is different. The Nedjar method is said to have converged when $\|\Delta T_i\|_\infty < \epsilon$, and corresponding results are presented in this section. The reason for this choice of stopping criterion is that results for a relative stopping criterion $\|\Delta T_i\|_\infty < \epsilon \|\Delta T_0\|_\infty$ are found to be up to the third or higher significant digit equal to those found using the absolute stopping criterion, but slightly more iterations are required, and thus more computational time. The Fachinotti method is said to have converged when $\|\Psi(T_i^{m+1})\|_\infty < \epsilon \|\Psi(T^m)\|_\infty$.

Although the solution methods and their corresponding stopping criterion are essentially different, we believe that the comparison presented in this section is valid. The reason is that for the given value of ϵ, the computed errors with respect to the similarity solution, in both the 2-norm and ∞-norm, are of the same order of magnitude. This argument holds for the temperature as function of time as well as position.

5.1 Results

The performance of the two presented methods is evaluated using two 1D test cases taken from Chun and Park[2]. Both test cases consider the melting of a single material. In the first test case, the physical parameters are taken to be equal and constant for both phases. This test case will be referred to as '*equal parameters*'. In test case '*unequal parameters*', the physical parameters are taken to be different, but constant, for each phase. The benefit of these two test cases is the existence of a corresponding analytical solution. For more details on these test problems we refer to Chun and Park[2].

The computations for the original test cases are performed on a spatial grid consisting of 100 elements. For the test problem 'equal parameters' the temperature as a function of time for both methods is plotted in Figure 2. Notice that the solution as computed using the method by Nedjar clearly shows 'staircasing', which is characteristic for enthalpy

methods. The temperature method exhibits a similar type of behavior.

For the test cases 'equal parameters' and 'unequal parameters', results with respect to the refinement of the spatial grid are listed in Tables 1 and 2, respectively. The tables clearly show that in general the error for the temperature as a function of time (error 1) is about ten times larger (in both norms) than the error for the temperature as a function position (error 2). In addition, the reduction of the errors is linear when the spatial grid size is doubled, as expected.

Clearly, the test problem 'unequal parameters' is computationally more demanding than the test case in which the physical parameters are taken to be equal for both phases. The computational load, expressed in the average number of (pseudo)-Newton iterations, and the total computational time, for the Nedjar method scales with the increase of the number of elements. For the temperature based method, the computational load hardly increases when the mesh is refined.

method	n	time (s)	av. #iters	x_m	error 1	error 2
Nedjar	100	12	28	0.600	12 (25)	0.89 (2.2)
	200	18	55	0.600	5.5 (13)	0.60 (2.0)
	400	44	116	0.575	2.6 (8.0)	0.43 (1.8)
	800	91	137	0.594	1.9 (3.1)	0.22 (0.70)
Fachinotti	100	10	3.2	0.601	8.1 (17)	1.3 (1.7)
	200	10	3.5	0.593	4.2 (7.1)	0.67 (0.98)
	400	13	4.0	0.589	2.2 (3.6)	0.38 (0.76)
	800	18	4.6	0.587	1.3 (2.1)	0.15 (0.19)

Table 1: Test case 'equal parameters'. The effect of refining the spatial grid. The errors 1 and 2 are given in both the 2-norm and $\infty-$norm (within brackets). The 'exact' position of the moving interface at $t = t_{\text{end}}$ is $x_m = 0.587$.

method	n	time (s)	av. #iters	x_m	error 1	error 2
Nedjar	100	107	11	0.700	11 (30)	0.98 (2.1)
	200	131	19	0.750	4.7 (18)	0.56 (2.0)
	400	223	36	0.725	2.0 (9.4)	0.31 (1.4)
	800	564	72	0.738	0.85 (5.3)	0.06 (0.64)
Fachinotti	100	102	3.0	0.748	2.1 (6.0)	0.49 (1.4)
	200	110	3.1	0.744	0.88 (3.2)	0.15 (0.39)
	400	128	3.5	0.743	0.41 (1.6)	0.08 (0.25)
	800	171	4.0	0.743	0.20 (0.75)	0.04 (0.19)

Table 2: Test case 'unequal parameters'. The effect of refining the spatial grid. The errors 1 and 2 are given in both the 2-norm and $\infty-$norm (within brackets). The 'exact' position of the moving interface at $t = t_{\text{end}}$ is $x_m = 0.742$.

An interesting observation can be made from Table 3. For problems, where the melting front moves very rapidly, i.e., the Stefan number $St \approx \mathcal{O}(10^2)$, the enthalpy based method seems to be the method of choice. However, for the phase-change materials that are used in optical rewritable recording, a Stefan number of $\mathcal{O}(10^{-3})$ is commonly found. These problems can thus best be resolved using the method of Fachinotti.

Stefan number St		$\approx 5 \times 10^{-4}$	$\approx 5 \times 10^{-2}$	$\approx 5 \times 10^{0}$	$\approx 5 \times 10^{2}$
total #Newton iterations	Fachinotti	2322	2829	4957	6603
	Nedjar	78947	43045	14396	6271
total time (s)	Fachinotti	23	29	45	58
	Nedjar	355	195	132	32

Table 3: Performance with respect to Stefan number St, $\epsilon = 10^{-3}$, $\Delta t = 2000$, $n = 800$, $t_{\text{end}} = 20$ days.

As a final test case, we consider the melting of a square region filled by a phase-change material, which on two sides is embedded by a non-melting material, see Figure 3. The material properties of the phase-change material are taken equal to those used in the first test case. For the embedding material, $\rho = 1$ kg/m^3, $C = 1{\times}10^6$ J/kg$^\circ C$, $\kappa = 0.5$ W/m$^\circ C$, $L = 2{\times}10^4$ J/kg and $T_m = 20\ ^\circ C$. Table 4 shows that the computational demand of the Fachinotti method does not increase as rapidly for smaller values of the tolerance ϵ then that of the Nedjar method. This is caused by the damping factor μ in the pseudo Newton iteration process.

In Figure 4, contour levels are plotted of the temperature within the composite domain. The figure illustrates the difference in the captured interface position. Although the moving interface, represented by contour level 5, is very smooth when using the temperature approach, Nedjar clearly shows oscillations.

		$\epsilon = 10^{-2}$	$\epsilon = 10^{-4}$	$\epsilon = 10^{-6}$
total #Newton iterations	Fachinotti	1734	2599	3376
	Nedjar	10107	46020	88964
total time (s)	Fachinotti	116	166	208
	Nedjar	266	1093	2030

Table 4: Computational load for the 2D multi-layer test problem for varying tolerance ϵ: $\Delta t = 2000$, $t_{\text{end}} = 20$ days.

6 CONCLUSIONS

Based on the results, the temperature based method seems to be the method of choice for small and medium range Stefan numbers. Not only can it easily be integrated into existing finite element codes for diffusion problems in composite domains, it also outperforms the enthalpy based method with respect to accuracy, stability and computational

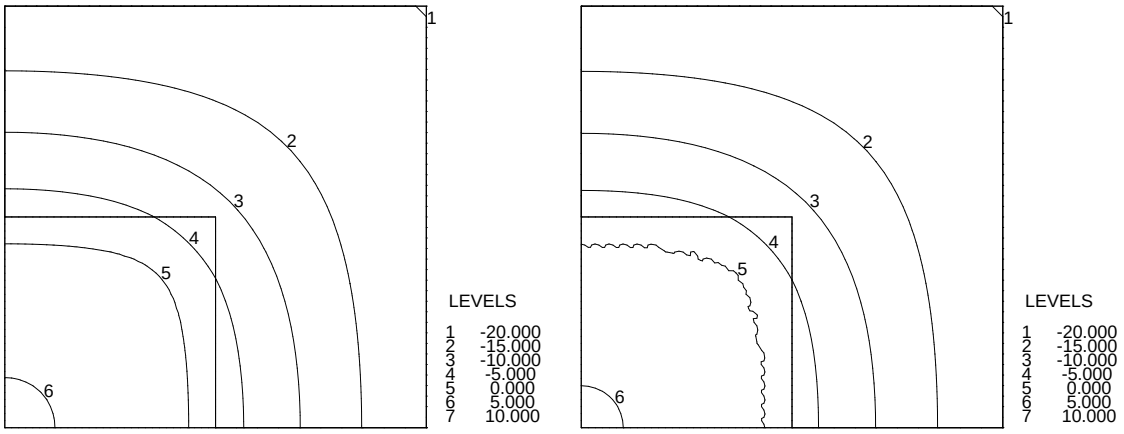

Fachinotti Nedjar

Figure 4: Results for the 2D test case. Fachinotti: no wiggles; Nedjar: wiggles, $\epsilon = 10^{-3}$, $\Delta t = 2000$, $t_{\text{end}} = 20$ days.

load. For melting problems with Stefan numbers of $\mathcal{O}(10^2)$ or larger, the enthalpy method might be the better choice.

REFERENCES

[1] J.H. Brusche, A. Segal and H.P. Urbach. Finite-element model for phase-change recording. *J. Opt. Soc. Am. A*, **22**, 773–786, (2005).

[2] C.K. Chun and S.O. Park. A fixed-grid finite-difference method for phase-change problems. *Numer. Heat Transfer, Part B*, **38**, 59–73, (2000).

[3] V.D. Fachinotti, A. Cardona and A.E. Huespe. A fast convergent and accurate temperature model for phase-change heat conduction. *Int. J. Numer. Meth. Engng.*, **44**, 1863–1884, (1999).

[4] B. Nedjar. An enthalpy-based finite element method for nonlinear heat problems involving phase change. *Comput. Struct.*, **80**, 9–21, (2002).